Supporting Information

Role of Molecular Dipoles in Charge Transport across Large Area Molecular Junctions Delineated using Isomorphic SAMs

Jiahao Chen,[1] Symon Gathiaka,[2] Zhengjia Wang,[1] Martin M. Thuo[1]*

[1]Department of Materials Science and Engineering, Iowa State University, 2220 Hoover Hall, Ames, IA 50011 USA

[2]School of Pharmacy and Pharmaceutical Science, University of California, San Diego, 9500 Gilman Drive, MC 0657, La Jolla, CA 92093-0657 (USA)

Experimental Section

Surface characterization and analysis: A Bruker Multi-Mode AFM was used in tapping mode to characterize the surface features of all surfaces. All samples were scanned immediately after the lift-off. The R_{rms} and PSD were analyzed by *Nanoscope* software automatically, while the bearing volume was analyze on sample image with 2μm x 2μm size. A Rigaku Ultima IV powder diffractometer were used to investigate the faceting of the substrate surface.

Preparion of Self-Assembled Monolayers (SAMs): Self-Assembled monolayers were prepared as previously reported.[1-5] Carboranethiols were dissolved in 200 proof ethanol to obtain 1.5mM solution. A template-stripped Au surface was rinsed and dried with nitrogen gas and then placed into a vial containing 5ml carboranethiol solution. The solution and the substrate were incubated overnight under inert atmosphere.

Measuring tunneling current: An EGaIn conical tip was prepared as previously reported [3, 4] and was gently used to contact the monolayer forming a junction. The junction was swept with ±0.5 V or ±1 V bias. Data analysis was performed using *LAJA*—a custom built, in-house, MATLAB code as previously reported.[6]

Calculation of molecular properties (molecules in free space): The electrostatic potential (ESP) maps were calculated using the Gaussian software package.[7] The geometries of the 3 isomers were optimized using density functional theory at the B3LYP level with the 6-311++g(2d,p) basis set. For comparison purposes, the complete basis set method (QBS-QB3) was also used and the dipole moments evaluated. Mulliken charges used for the electrostatic potential mapping were computed from the single point structures of the CBS-QB3 geometry at the Hartree-Fock level with the 6-31+G(d) basis set.

Background

Molecular electronics offers the prospect to engineer wave-function, hence conductance, in small (nanometer-sized) devices through synthetic chemistry leading to, potentially, great advances in neoteric single-molecule electronic devices. This promise is driven by advances in synthesis that allow for control over stereo-electro-chemical properties of molecules. Self-assembled monolayers (SAMs) formed on metal surfaces have been used to study charge transport properties of a collection of ordered single molecules, which are commonly referred to as large-area molecular junctions. The molecular junction can be simplified into resistors in series, where a typical eutectic gallium based junction consists of the resistance of the SAM (R_{SAM}) and the contact resistance (R_C). The charge transport rate is dependent on the length of the tunneling path (barrier width), which is related to the length of the molecule, while the mechanism of charge transport is dependent on the position of the molecules energy states relative to the vacuum (barrier height) and the Fermi level, E_F, of the electrodes.[8] The simplified Simmons equation (Equation S1) is commonly used to describe the rate of charge transport and highlights the need for a constant barrier width in a comparative study of electronic properties of the SAM;

$$J = J_0 e^{-\beta d} \qquad \text{S1}$$

Where J (A/cm^2) is the current density, J_0 is the injection current, β is the decay constant, and d is the barrier width.

This interdependence, we believe, has led to some ambiguities, especially across different platforms or groups. For example; several recent reports show an odd-even effect (in terms of

non-H atoms in the SAM) on the rate of charge transport through monolayers[4, 5, 9] or organic field-effect transistors (OFETs)[4, 5, 9, 10] while others do not.[5, 11] Jiang et al.[9] recently reported the origin of odd-even effect in tunneling rates across n-alkanethiolate SAMs, observing that the contact resistance is different between odds and evens. This variance indicates that the orientation of the top moiety affects the charge transport rate, to a small extent. Others, however, have indicated that a "small" perturbation to the electronic nature of the "saturated" molecules, such as H-bonding and polarity of the head group,[11-13] anchoring group,[14, 15] and backbone,[3] has little or no observable effect on the rate of charge transport. These two sets of studies do not resolve the role of a moiety's dipole in charge tunneling, the latter being complicated by associated changes in the SAM with changes in molecule-structure.

Dipole moments have, however, been implicated in modifying the charge transport properties of SAMs manifesting in effects like rectification, quantum confinement or perturbing the overall rate of charge transport or associated mechanisms.[16-18] Some of these phenomena is associated with the potential for molecular dipoles to significantly tilt the barrier allowing transition from direct tunneling to Fowler-Nordheim tunneling (Figure S1) and this bias-dependent behavior can be captured through transition voltage spectroscopy (TVS) as the transition voltage (V_T) as shown below (Figure S1)

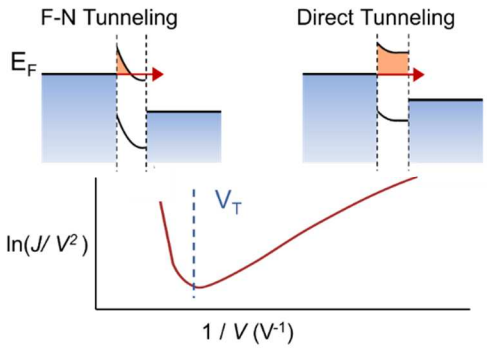

Figure S1. Illustration of the transition from direct tunnelling to Fowler-Nordheim tunnelling at transition voltage.

Charge transport across molecules is usually fitted to the simplified Simmon's model a (Equation S1), and, in most case, the decay constant, β, is associated with barrier height ϕ, as in Eq. 2;

$$\beta = 2\sqrt{\frac{2m\alpha(\phi - \frac{qV}{2})}{\hbar^2}} \quad (2)$$

Where m is the effective mass of an electron ($0.9m_e$; kg), α is a unitless fitting parameter for non-rectangular barrier compensation, ħ is Plank's constant divided by 2π (J·s), ϕ is the barrier height, qV is the energy level change due applied field.

From this relation, we can infer that, at least under positive bias, β decreases as $(\phi - \frac{qV}{2})$—since the magnitude of the effective energy barrier for charge injection at the metal-molecule interface decreases. This dependence is largely due to metallic orbitals and molecular orbitals coming into resonance. At the metal/molecule interface, significant band bending occurs due to Fermi-level pinning/ Charge Neutrality Level (CNL) alignment for weakly physisorbed molecule/metal interface.[19-22] The case for chemisorbed interface is much more complicated, due to particle charge transfer across the bond, resultant surface dipoles, σ–σ* hyperconjugation, and delocalization of orbitals between metal and molecules. [23, 24] It is therefore important to compare

current densities from equivalent positive and negative biases, or deploy isomorphic SAMs (no structural differences) where the decay parameter is not a necessary variable to consider as there are no height changes.

Differences in tunneling rate can also be due to changes in total work function (surface potential), $\Delta\Phi_{total}$, at the metal surface, which can be induced by chemical bond formation ($\Delta\Phi_{chem}$), metal surface dipole/work function exchange ($\Delta\Phi_{m,dipole}$) and molecular dipole ($\Delta\Phi_{mol,dipole}$), as shown in Eq. S3;[24]

$$\Delta\Phi_{total} = \Delta\Phi_{chem} + \Delta\Phi_{m,dipole} + \Delta\Phi_{mol,dipole} \quad \text{(S3)}$$

Recent theoretical work reported by Mete et al.[25] shows that the work function change of Au surface upon M1 deposition is negligible (an increase of 0.05eV), while the change of work function with M9 deposition is much more significant (a decrease of 0.70eV). Based on this observation, we can anticipate that there will be significant differences in charge tunneling when the junction symmetry plays a significant role or this change in the work function significantly tilts the barrier towards a change into classical physics based transport as opposed to direct tunneling where only the nature of the barrier plays a significant role. This difference in work function may also lead to differences in contact resistance or charge injection into the metal.

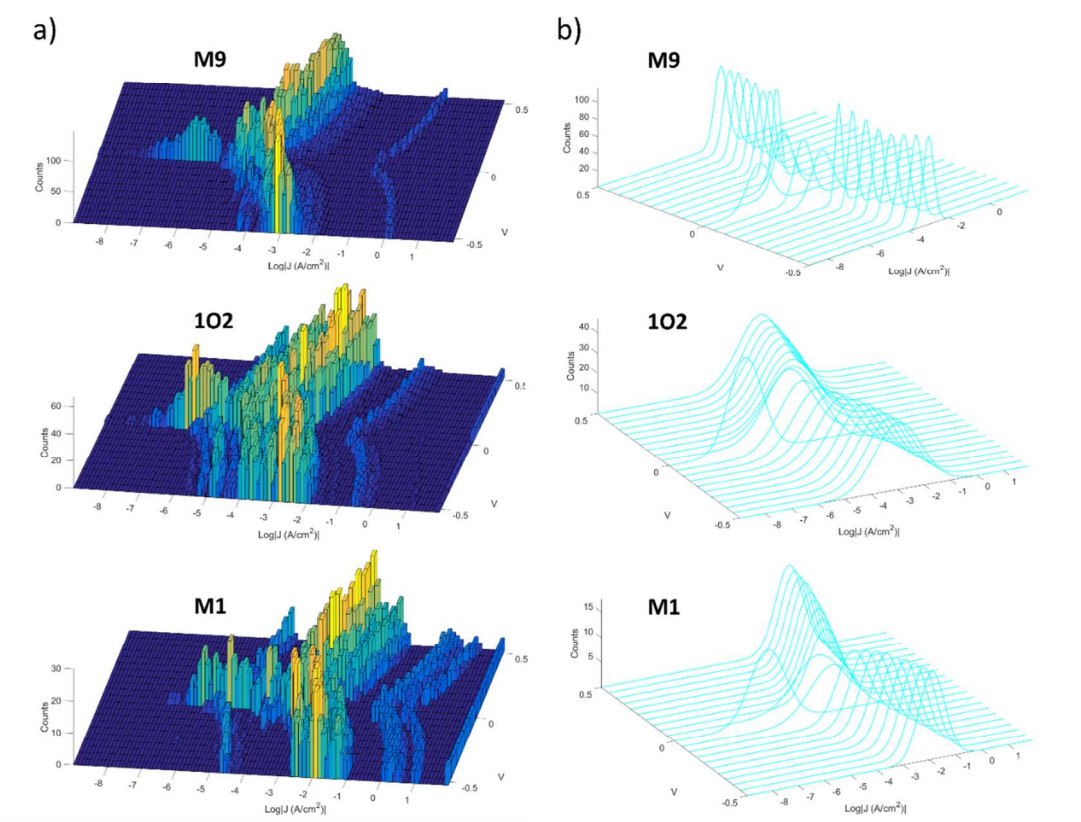

Figure S2. The raw data was analyzed by *LAJA*. a) The 3D histogram and, b) the Gaussian fit curve plots of tunneling current across M1, M9 and 1O2 carboranethiol derived junctions.

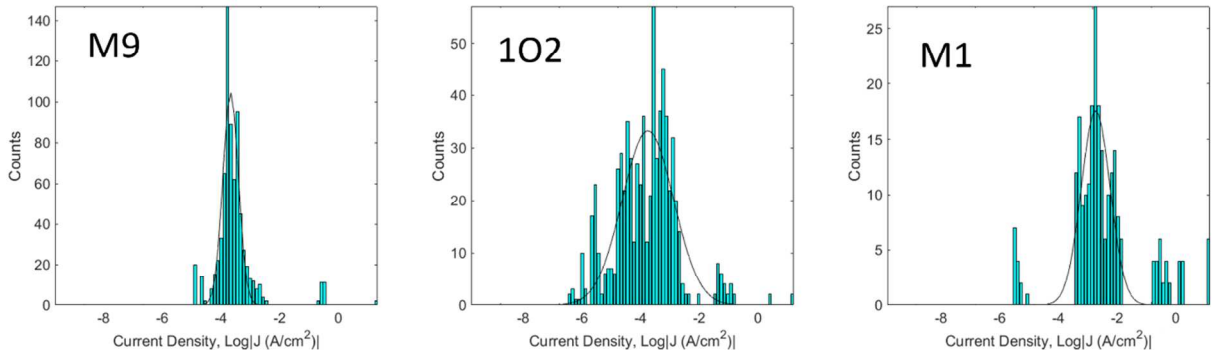

Figure S3. The histogram of tunneling current at -0.5 V across three carboranethiol derived junctions.

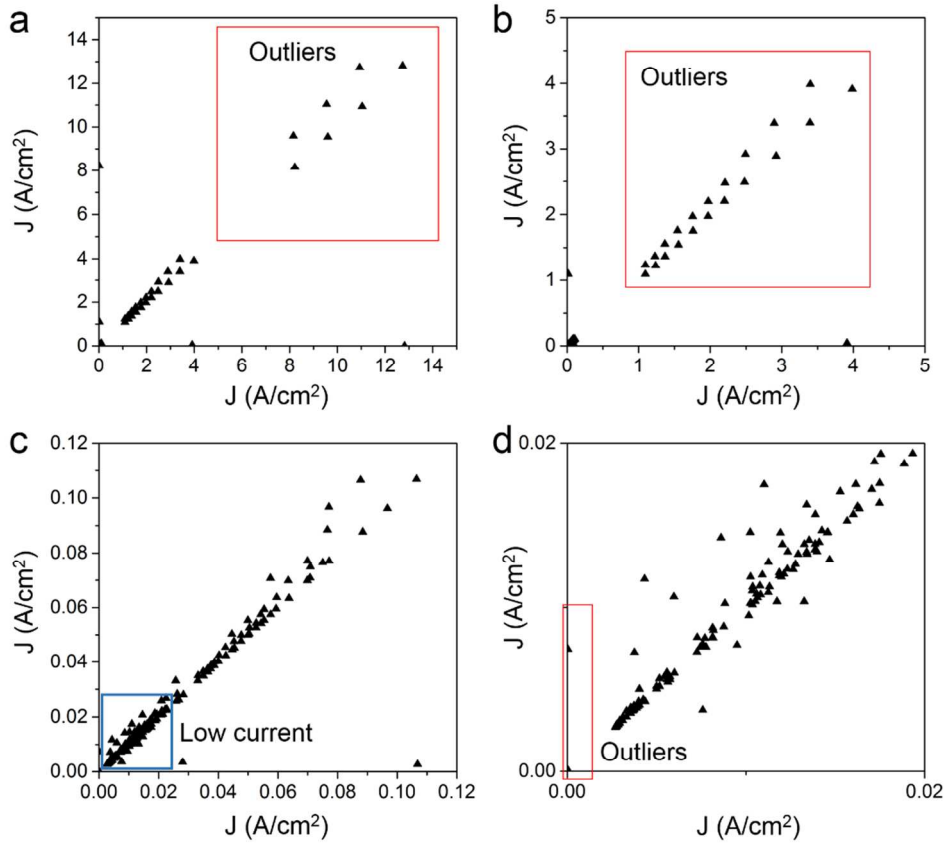

Figure S4. The lag plots showing the current density at -0.5V for all junctions of M1. The outliers can be easily distinguished from the main part of the data.

The lag plots show the current density measurements against the next measured current density. Here the lag plots show a linear correlations of the measured results. From this, we argue that there is no secondary effect (over time) during the measurements, such as oscillation of tip configurations.

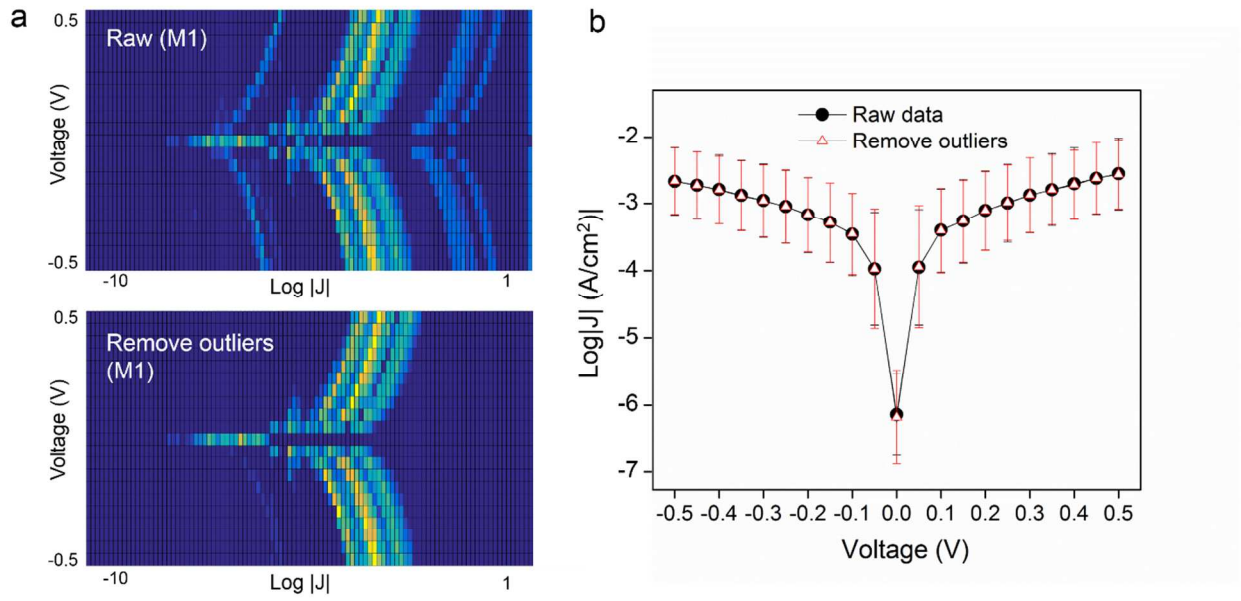

Figure S5. The heap-map of charge transport data across M1 junctions before removing and after removing the outliers. The Gaussian mean values calculated from raw data and "purified" data show no significant differences.

Table S1. Transition voltage of three molecules estimated at positive bias and negative bias.

Transition voltage	*At positive bias [Vt(+)]*	*At negative bias [Vt (-)]*	*Ratio of [Vt(+)]/[Vt (-)]*
M1	0.50	0.93	0.54
M9	0.43	0.74	0.54
1O2	0.41	0.71	0.56

From the F-N plot, the transition voltage can be estimated by replotting the 1st derivative of the F-N curves.

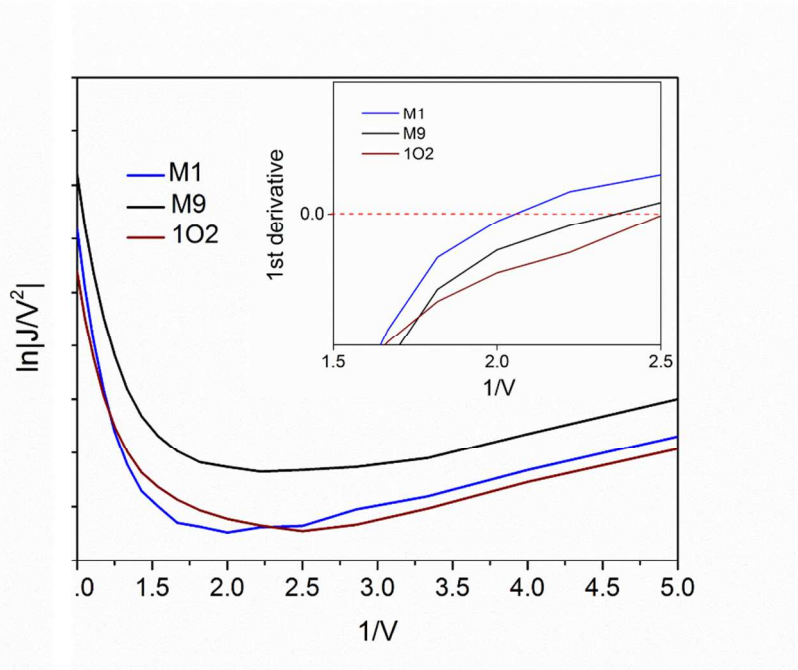

Figure S6. The F-N plots for three molecules for forward and reverse bias. There is distinct transition at forward bias at certain transition voltage (V_T) for all molecules. For reverse bias, no distinct transition was observed from direct tunneling to F-N tunneling.

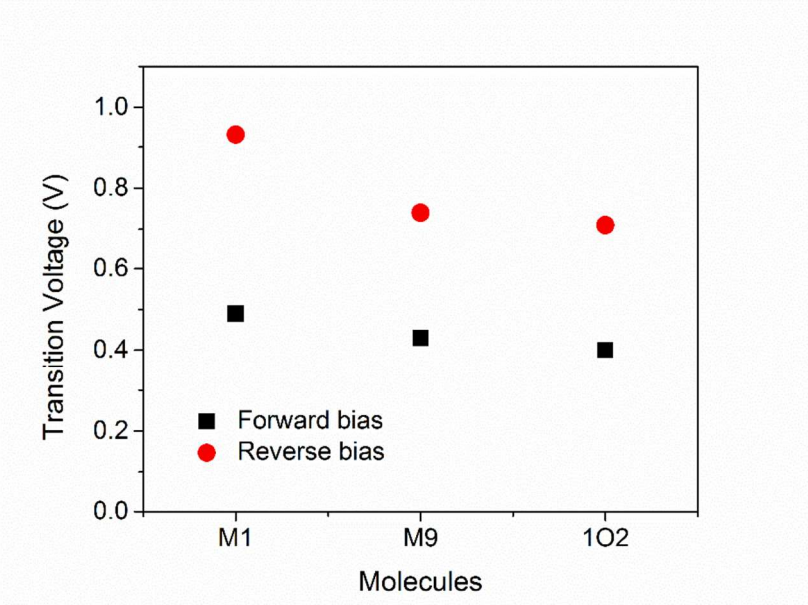

Figure S7. The transition voltage of the junctions (M1, M9 and 1O2) shows significant difference at forward bias and reverse bias.

Table S2. The measured rectification ratio (RR) of current at +1V to that at -1V.

	Gaussian mean	*Average*
M1	13.0x10^(±0.406)	13.7 ± 4.8
M9	10.3x10^(±0.397)	9.4 ± 3.3
1O2	6.4x10^(±0.337)	6.4 ± 2.1

We estimated the ratio by comparing the Gaussian mean values of current density at +1V and at -1V. RR= logJ(+1V)/logJ(-1V) We also estimated this through averaging the rectification ratio between +1V and -1V of each measurement traces. RR= Ave[J(+1V)/J(-1V)]. Those two method gives very similar average values, though the errors from these two methods are much more different.

Rectification in charge transport

The alignment of the dipole with electron flow affects tunneling rates, and may also affect asymmetric charge transport across the barrier due to directional orientation of the dipole moment, that is; direction of low to high electron density may affect charge injection rates.[19, 26, 27] When the top-electrode is negatively biased, the direction of the molecular dipole in M9, for example, is misaligned to the flow of the current and as such charge injection is energetically uphill compared to 1O2 where the field gradient is aligned to the direction of the molecular dipole moment.[16, 26, 27] Accordingly, M9 and 1O2 junctions with aligned dipoles are expected to rectify current, in the opposite directions, while for M1, the rectification should be negligible. One caveat with this observation is that the sensitivity of EGaIn top-electrodes to such subtle molecular changes has not been evaluated and neither is the role of non-bonding orbitals.

Under ±1V applied bias, significant asymmetric transport was observed with higher currents at +1V. We observed that the rectification ratio was independent of the direction of the dipoles. The average rectification ratio across the three molecules was 14, 9 and 6 for M1, M9 and 1O2, respectively (Table S1). Unlike in previous studies with aromatic cores,[16] carboranes- with their pseudo-aromatic structures, do not show a dipole-dependent trend in their rectification. The M1 carborane shows larger rectification even though the dipole moment is orthogonal to the surface normal. Since the rectification ratios are low, we exercise caution in their interpretation. To further delineate the effect of dipole on the charge tunneling characteristics of these cage molecules, transition voltage spectroscopy was obtained. Variance in transition voltage (V_T) has been shown to correlate well with molecular dipoles for SAMs of similar barrier widths..[28, 29] The V_T for all molecules was analyzed from F-N plots as previously reported (Figure S5).[16]

When the top-electrode is under a positive bias, higher currents were observed leading to rectification and so were the V_T.[30] Trends in V_T mirror trends in the rectificantion ratios.

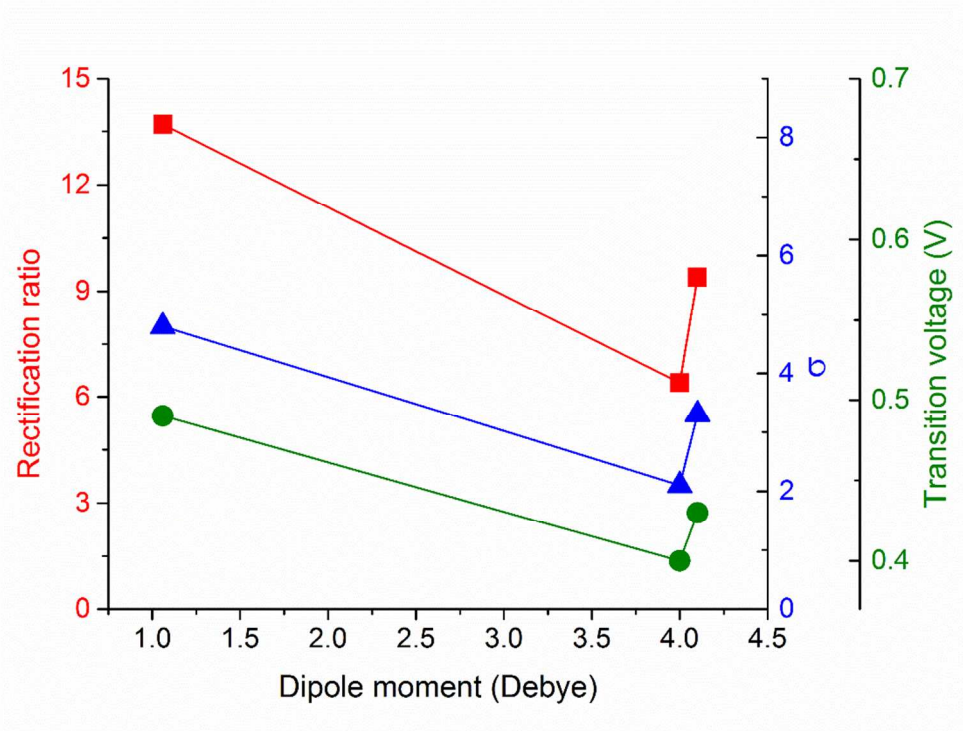

Figure S8. The correlation between the dipole and the average rectification ratio (RR), its corresponding deviation (σ_{RR}) and the transition voltage show similar trends.

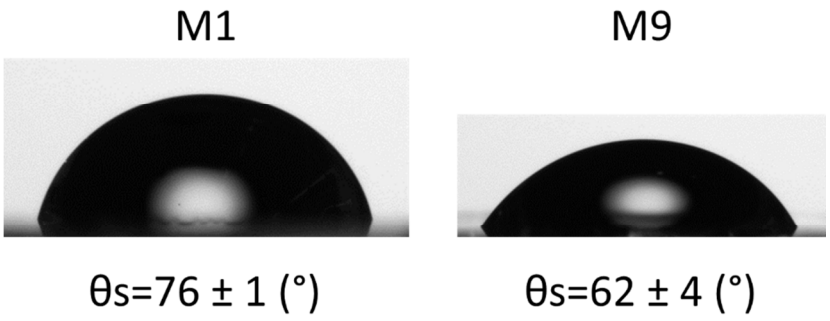

Figure S9. Static contact angle of water on M1 and M9 formed on Au surface. The contact angle value is comparable to literature as advancing and receding contact angle.[31]

References

1. Chen, J.; Wang, Z.; Oyola-Reynoso, S.; Gathiaka, S. M.; Thuo, M. *Langmuir* **2015,** 31, (25), 7047-7054.
2. Newcomb, L. B.; Tevis, I. D.; Atkinson, M. B.; Gathiaka, S. M.; Luna, R. E.; Thuo, M. *Langmuir* **2014,** 30, (40), 11985-11992.
3. Thuo, M. M.; Reus, W. F.; Simeone, F. C.; Kim, C.; Schulz, M. D.; Yoon, H. J.; Whitesides, G. M. *J. Am. Chem. Soc.* **2012,** 134, (26), 10876-10884.
4. Thuo, M. M.; Reus, W. F.; Nijhuis, C. A.; Barber, J. R.; Kim, C.; Schulz, M. D.; Whitesides, G. M. *J. Am. Chem. Soc.* **2011,** 133, (9), 2962-2975.
5. Baghbanzadeh, M.; Simeone, F. C.; Bowers, C. M.; Liao, K.-C.; Thuo, M.; Baghbanzadeh, M.; Miller, M. S.; Carmichael, T. B.; Whitesides, G. M. *J. Am. Chem. Soc.* **2014,** 136, (48), 16919-16925.
6. Sporrer, J.; Chen, J.; Wang, Z.; Thuo, M. M. *J. Phys. Chem. Lett.* **2015,** 6, (24), 4952-4958.
7. Frisch, M. J.; Trucks, G. W.; Schlegel, H. B.; Scuseria, G. E.; Robb, M. A.; Cheeseman, J. R.; Scalmani, G.; Barone, V.; Mennucci, B.; Petersson, G. A.; Nakatsuji, H.; Caricato, M.; Li, X.; Hratchian, H. P.; Izmaylov, A. F.; Bloino, J.; Zheng, G.; Sonnenberg, J. L.; Hada, M.; Ehara, M.; Toyota, K.; Fukuda, R.; Hasegawa, J.; Ishida, M.; Nakajima, T.; Honda, Y.; Kitao, O.; Nakai, H.; Vreven, T.; Montgomery Jr., J. A.; Peralta, J. E.; Ogliaro, F.; Bearpark, M. J.; Heyd, J.; Brothers, E. N.; Kudin, K. N.; Staroverov, V. N.; Kobayashi, R.; Normand, J.; Raghavachari, K.; Rendell, A. P.; Burant, J. C.; Iyengar, S. S.; Tomasi, J.; Cossi, M.; Rega, N.; Millam, N. J.; Klene, M.; Knox, J. E.; Cross, J. B.; Bakken, V.; Adamo, C.; Jaramillo, J.; Gomperts, R.; Stratmann, R. E.; Yazyev, O.; Austin, A. J.; Cammi, R.; Pomelli, C.; Ochterski, J. W.; Martin, R. L.; Morokuma, K.; Zakrzewski, V. G.; Voth, G. A.; Salvador, P.; Dannenberg, J. J.; Dapprich, S.; Daniels, A. D.; Farkas, Ö.; Foresman, J. B.; Ortiz, J. V.; Cioslowski, J.; Fox, D. J. *Gaussian 09*, Gaussian, Inc.: Wallingford, CT, USA, 2009.
8. Song, H.; Kim, Y.; Jeong, H.; Reed, M. A.; Lee, T. *The Journal of Physical Chemistry C* **2010,** 114, (48), 20431-20435.
9. Jiang, L.; Sangeeth, C. S.; Nijhuis, C. A. *J. Am. Chem. Soc.* **2015,** 137, (33), 10659-10667.
10. Akkerman, H. B.; Mannsfeld, S. C.; Kaushik, A. P.; Verploegen, E.; Burnier, L.; Zoombelt, A. P.; Saathoff, J. D.; Hong, S.; Atahan-Evrenk, S.; Liu, X. *J. Am. Chem. Soc.* **2013,** 135, (30), 11006-11014.
11. Yoon, H. J.; Shapiro, N. D.; Park, K. M.; Thuo, M. M.; Soh, S.; Whitesides, G. M. *Angewandte Chemie* **2012,** 124, (19), 4736-4739.
12. Yoon, H. J.; Bowers, C. M.; Baghbanzadeh, M.; Whitesides, G. M. *J. Am. Chem. Soc.* **2013,** 136, (1), 16-19.
13. Mirjani, F.; Thijssen, J. M.; Whitesides, G. M.; Ratner, M. A. *ACS nano* **2014,** 8, (12), 12428-12436.
14. Fracasso, D.; Kumar, S.; Rudolf, P.; Chiechi, R. C. *Rsc Advances* **2014,** 4, (99), 56026-56030.
15. Liao, K. C.; Yoon, H. J.; Bowers, C. M.; Simeone, F. C.; Whitesides, G. M. *Angewandte Chemie International Edition* **2014,** 53, (15), 3889-3893.
16. Kovalchuk, A.; Abu-Husein, T.; Fracasso, D.; Egger, D. A.; Zojer, E.; Zharnikov, M.; Terfort, A.; Chiechi, R. C. *Chemical Science* **2016,** 7, (1), 781-787.
17. Castañeda Ocampo, O. E.; Gordiichuk, P.; Catarci, S.; Gautier, D. A.; Herrmann, A.; Chiechi, R. C. *J. Am. Chem. Soc.* **2015,** 137, (26), 8419-8427.
18. Carlotti, M.; Kovalchuk, A.; Wächter, T.; Qiu, X.; Zharnikov, M.; Chiechi, R. C. *Nature Communications* **2016,** 7.
19. Liu, Z.; Kobayashi, M.; Paul, B. C.; Bao, Z.; Nishi, Y. *Phys. Rev. B* **2010,** 82, (3), 035311.
20. Helander, M.; Wang, Z.; Qiu, J.; Lu, Z. *Applied Physics Letters* **2008,** 93, (19), 193310.
21. McCreery, R. L.; Yan, H.; Bergren, A. J. *Phys. Chem. Chem. Phys.* **2013,** 15, (4), 1065-1081.
22. Heimel, G.; Romaner, L.; Zojer, E.; Bredas, J.-L. *Accounts of Chemical Researchc* **2008,** 41, (6), 721-729.
23. Xue, Y.; Datta, S.; Ratner, M. A. *J. Chem. Phys.* **2001,** 115, (9), 4292-4299.
24. Karthäuser, S. *Journal of Physics: Condensed Matter* **2010,** 23, (1), 013001.

25. Mete, E.; Yılmaz, A.; Danışman, M. F. *Phys. Chem. Chem. Phys.* **2016,** 18, (18), 12920-12927.
26. Mafé, S.; Manzanares, J. A.; Reiss, H. *J. Appl. Phys.* **2011,** 109, (4), 044302-044302-6.
27. Manzanares, J. A.; Cervera, J.; Mafé, S. *J. Phys. Chem. C* **2011,** 115, (14), 6980-6985.
28. Jia, C.; Guo, X. *Chem. Soc. Rev.* **2013,** 42, (13), 5642-5660.
29. Beebe, J. M.; Kim, B.; Gadzuk, J.; Frisbie, C. D.; Kushmerick, J. G. *Phys. Rev. Lett.* **2006,** 97, (2), 026801.
30. Araidai, M.; Tsukada, M. *Physical Review B* **2010,** 81, (23), 235114.
31. Hohman, J. N.; Zhang, P.; Morin, E. I.; Han, P.; Kim, M.; Kurland, A. R.; McClanahan, P. D.; Balema, V. P.; Weiss, P. S. *ACS nano* **2009,** 3, (3), 527-536.